# General Information on the Wind Tunnel Data from the CRM-NLF Test

## Table of Contents


| | |
|---|---|
| 1. National Transonic Facility General Information | Page 2 |
| 2. Reference Parameters | Page 4 |
| 3. Wing Planform | Page 5 |
| 4. Transition Visualization Technique | Page 6 |
| 5. Boundary Layer Transition Specifications | Page 8 |
| 6. Static Pressure Instrumentation | Page 10 |
| 7. Semispan Model Standoff | Page 13 |
| 8. Data Correction Information | Page 14 |
| 9. Freestream Disturbance Intensity Measurements | Page 15 |



CRM-NLF Point of Contact:
Michelle Lynde <michelle.n.lynde@nasa.gov>

# 1. National Transonic Facility General Information

The National Transonic Facility (NTF) is a fan-driven, closed-circuit, continuous-flow, cryogenic pressurized wind tunnel (schematic shown in Figure 1.1). The test section is approximately 8.2 feet square and 25 feet long with 12 longitudinal slots and 14 reentry flaps in the top and bottom walls to prevent the flow from choking at near-sonic conditions. The nominal test section configuration possesses six slots in the top wall and six slots in the bottom, with a total bleed-through capacity of six percent.

This test was completed exclusively in nitrogen mode and almost exclusively at one nominal Mach number, namely Mach 0.86. Figure 1.2 shows the test conditions superimposed on the tunnel test envelope at Mach 0.86. While this envelope doesn't capture all the test conditions achieved during this test, it captures the primary conditions of interest at various chord Reynolds numbers. The specific tunnel conditions are listed with the data for each point released on the website.

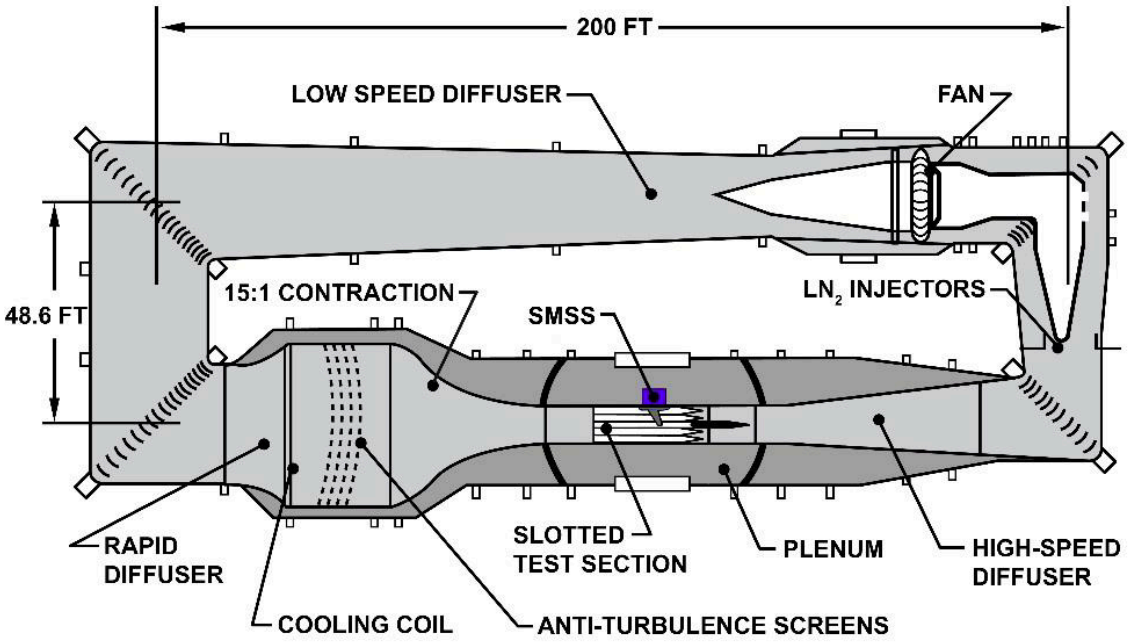


**Figure 1.1 Schematic of the National Transonic Facility.**

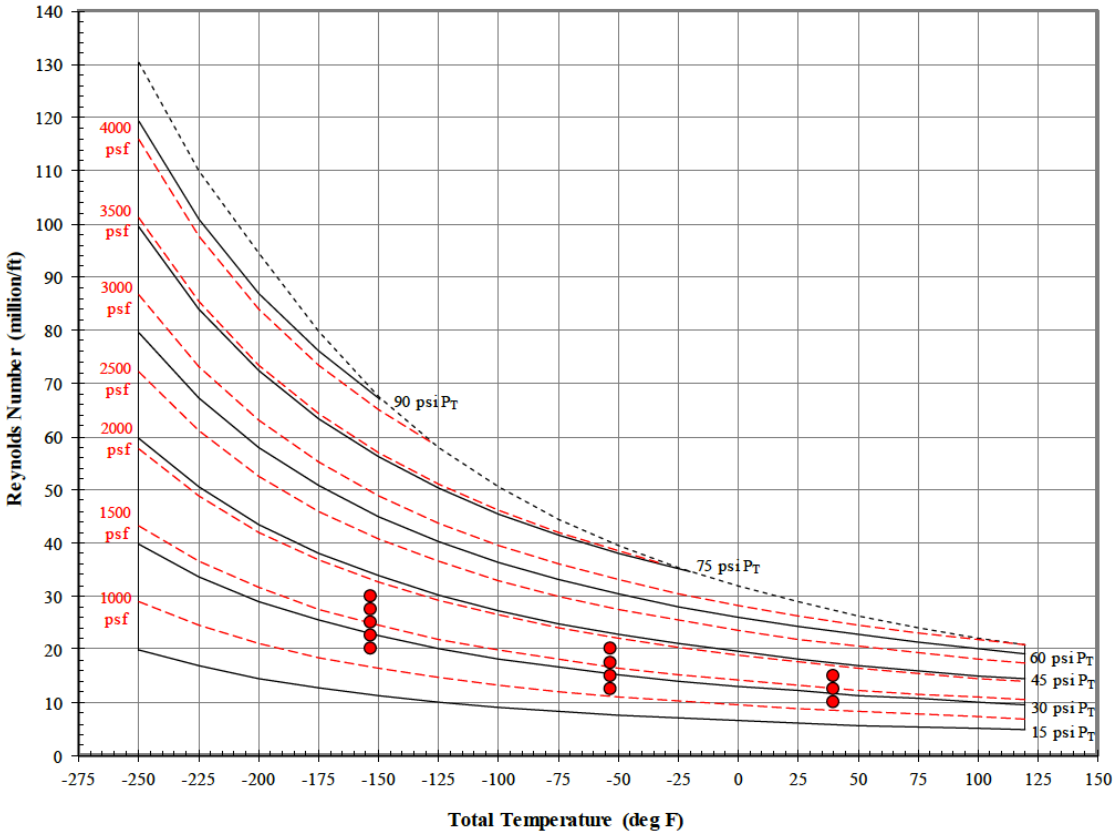


**Figure 1.2 Test Envelope at Mach 0.86 with Primary Test Conditions Identified.**

# 2. Reference Parameters

**Table 2.1 Model-Scale Reference Parameters.**

| | |
|---|---|
| Model Scale | 5.2% |
| Reference Area | 5.584 sq. ft. |
| Reference Chord | 14.342 in. |
| Semi-span | 60.151 in. |
| Leading-Edge Sweep (Outboard of LE curve) | 37.3 deg. |

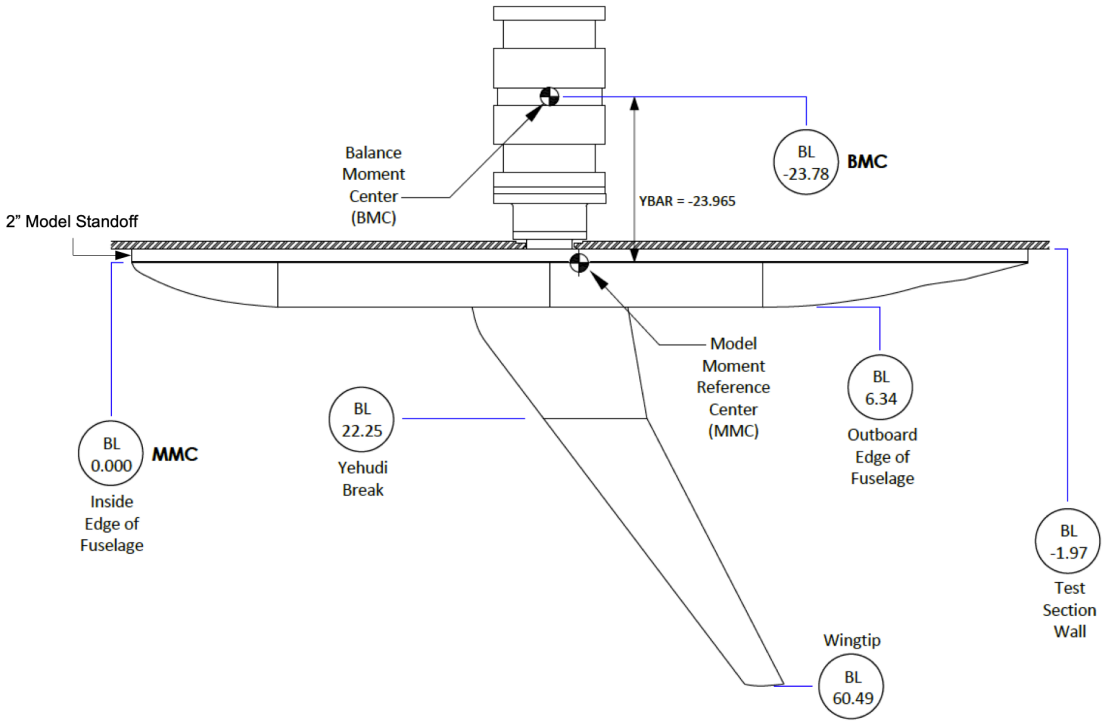


**Figure 2.1 Planform View of the CRM-NLF Model.**

# 3. Wing Planform

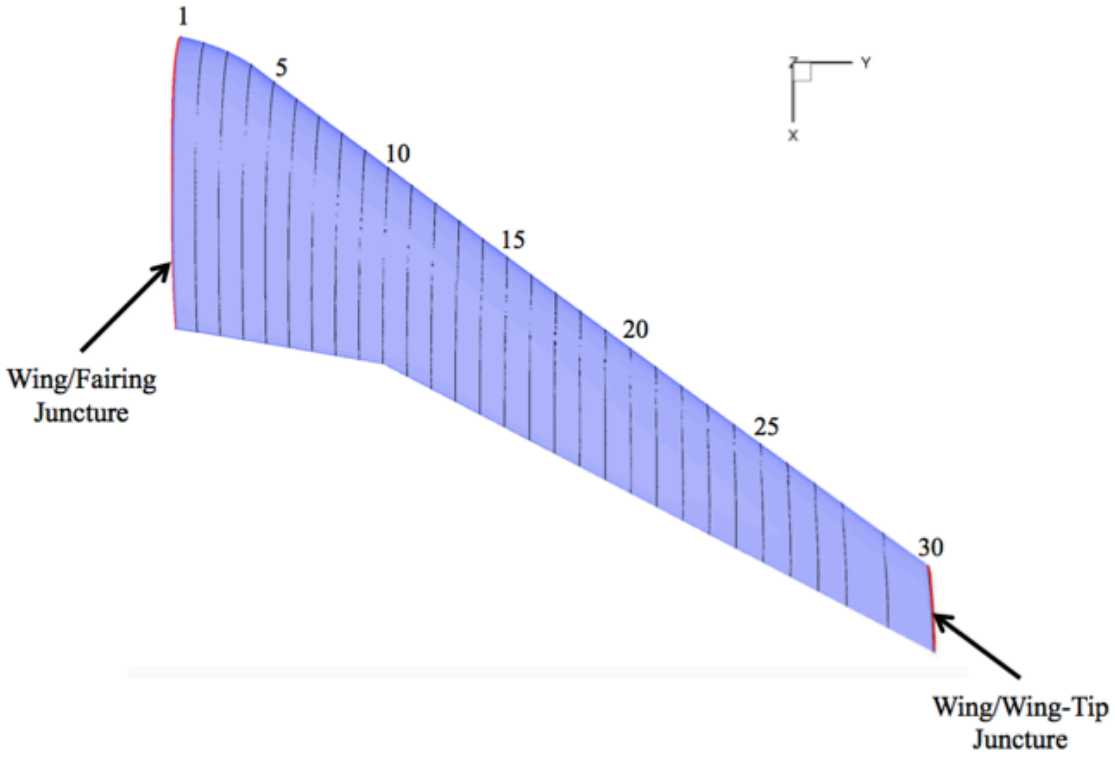


**Figure 3.1 Wing Planform with Wing Stations.**

**Table 3.1 Model-Scale Leading-Edge Coordinates of Wing Stations.**

| Station | $X_{LE}$ [in.] | $Y_{LE}$ [in.] | $Z_{LE}$ [in.] | Chord [in.] | Station | $X_{LE}$ [in.] | $Y_{LE}$ [in.] | $Z_{LE}$ [in.] | Chord [in.] |
|---|---|---|---|---|---|---|---|---|---|
| 1 | 53.566 | 6.253 | 9.116 | 22.285 | 16* | 71.988 | 33.083 | 9.930 | 12.210 |
| 2 | 53.969 | 7.976 | 9.011 | 22.136 | 17 | 73.362 | 34.888 | 10.087 | 11.768 |
| 3* | 54.627 | 9.782 | 8.944 | 21.778 | 18 | 74.736 | 36.692 | 10.263 | 11.327 |
| 4 | 55.616 | 11.587 | 8.934 | 21.103 | 19* | 76.110 | 38.497 | 10.460 | 10.885 |
| 5 | 56.971 | 13.365 | 8.973 | 20.063 | 20 | 77.484 | 40.301 | 10.664 | 10.443 |
| 6* | 58.327 | 15.144 | 9.039 | 19.022 | 21 | 78.858 | 42.106 | 10.885 | 10.001 |
| 7 | 59.681 | 16.922 | 9.115 | 17.982 | 22* | 80.232 | 43.910 | 11.120 | 9.560 |
| 8 | 61.034 | 18.700 | 9.187 | 16.942 | 23 | 81.606 | 45.715 | 11.359 | 9.118 |
| 9 | 62.389 | 20.478 | 9.253 | 15.901 | 24 | 82.980 | 47.519 | 11.608 | 8.676 |
| 10* | 63.743 | 22.256 | 9.320 | 14.861 | 25* | 84.354 | 49.324 | 11.868 | 8.235 |
| 11 | 65.117 | 24.061 | 9.396 | 14.419 | 26 | 85.728 | 51.128 | 12.138 | 7.793 |
| 12 | 66.491 | 25.865 | 9.496 | 13.977 | 27 | 87.102 | 52.933 | 12.415 | 7.351 |
| 13* | 67.865 | 27.670 | 9.599 | 13.535 | 28* | 88.476 | 54.738 | 12.704 | 6.909 |
| 14 | 69.239 | 29.474 | 9.691 | 13.094 | 29 | 90.456 | 57.338 | 13.168 | 6.273 |
| 15 | 70.613 | 31.279 | 9.802 | 12.652 | 30 | 92.598 | 60.151 | 13.719 | 5.584 |

*Pressure orifice row at this station

# 4. Transition Visualization Technique

Transition visualization images were acquired with Temperature Sensitive Paint (TSP). A resistive carbon-based heating layer was applied to the model beneath the TSP to provide the required temperature gradient to visualize regions of laminar/turbulent flow. Figure 4.1 illustrates the layers of paint used in this test. The heating layer produces a 5 – 10 °F increase in model surface temperature across the wing. On the upper surface of the wing, a grid was drawn on the top layer of paint to help identify the transition location in the images, seen in Figure 4.2. The chordwise lines are drawn at the 9 pressure rows ($Y/Y_{tip}$ = 0.163, 0.252, 0.370, 0.460, 0.550, 0.640, 0.730, 0.820, and 0.910) and the spanwise lines are drawn at 4 x/c locations (x/c = 0.20, 0.30, 0.40, and 0.50). Black circles were added across the span of the wing for image registration purposes.

During testing, the top layer of paint was frequently sanded and polished to maintain a high-quality finish. The paint thickness and surface roughness were measured at several chordwise and spanwise locations on the upper surface both before and after testing. These measurements (in mils or thousands of an inch) are recorded in Table 4.1.

All TSP images released on the website used the resistive carbon-based heating layer. Images were acquired at 2 Hz during 30 second data points. The images provided on the website have been averaged across the data acquisition period and post-processed using the Contrast Limited Adaptive Histogram Equalization (CLAHE) technique to enhance the image quality.

The carbon-based heating layer used electrical leads that were routed to the conductive strips internally through the wing to provide the required power to heat the model. The 18-gauge wires exited the internal channel and reached the surface at the 8 locations as specified in Table 4.2 and illustrated on the planform views in Figure 4.3.

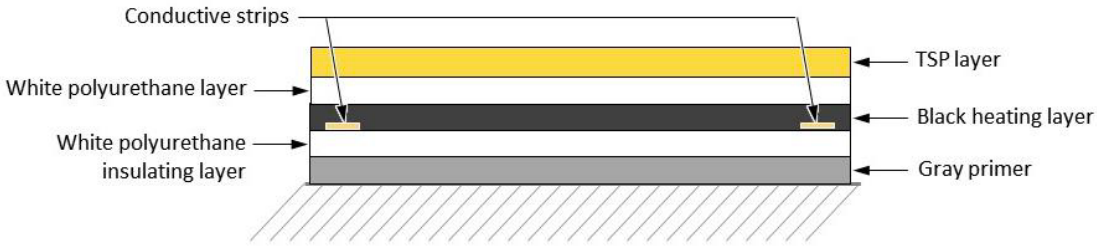


**Figure 4.1 Paint Layers on Wing.**

**Table 4.1 Paint Measurements.**

| Measurement | Location | Average Value Prior to Testing | Average Value After Testing |
|---|---|---|---|
| Thickness | Inboard | 16.35 mils | 15.48 mils |
| | Midspan | 12.15 mils | 11.80 mils |
| | Outboard | 10.83 mils | 10.62 mils |
| Roughness | Leading Edge | 1.64 µin | 1.10 µin |
| | 50% Chord | 0.90 µin | 0.83 µin |

**Figure 4.2 Photo of the CRM-NLF Wing After Final Paint Application.**

**Table 4.2 Surface Locations of Electrical Leads.**

| Location | X [in.] | Y [in.] | Surface | Hole Diameter [in.] |
|---|---|---|---|---|
| A | 74.153 | 8.282 | Upper & Lower | 0.090 |
| B | 77.925 | 23.556 | Upper & Lower | 0.090 |
| C | 83.797 | 34.533 | Upper & Lower | 0.090 |
| D | 89.718 | 45.510 | Upper & Lower | 0.090 |

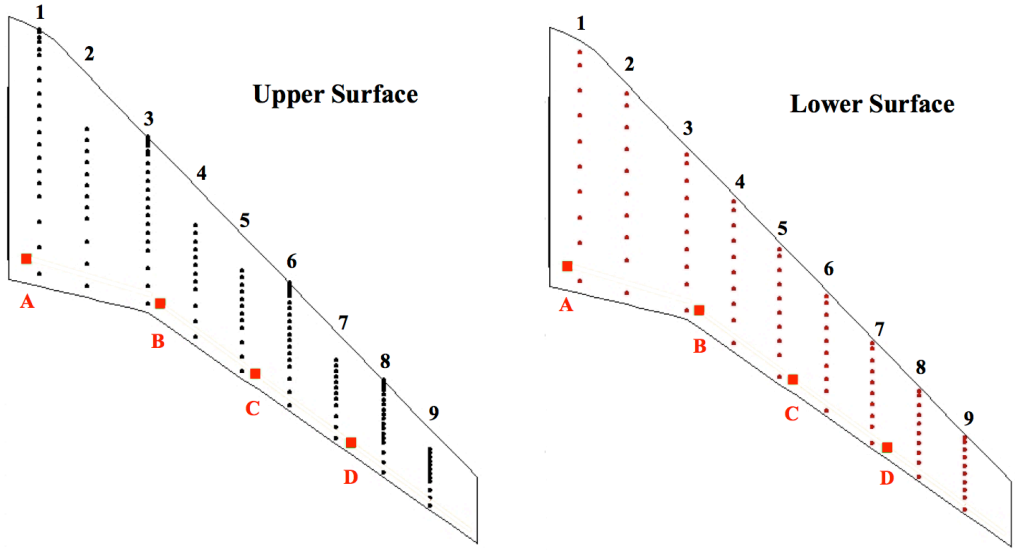


**Figure 4.3 Electrical Lead Surface Locations (Red Squares).**

# 5. Boundary Layer Transition Specifications

Self-adhesive trip dots were used to cause boundary layer transition on the lower surface of the wing and the fuselage. The trip dot dimensions are listed in Table 5.1. The locations of the trip dots are illustrated in Figures 5.1 and 5.2.

**Table 5.1 Trip Dot Dimensions.**

| Location | Diameter [in.] | Height [in.] | Spacing [in.] (Center to Center) |
|---|---|---|---|
| Wing Lower Surface | 0.05 | 0.002 | 0.10 |
| Fuselage Nose | 0.05 | 0.004 | 0.10 |

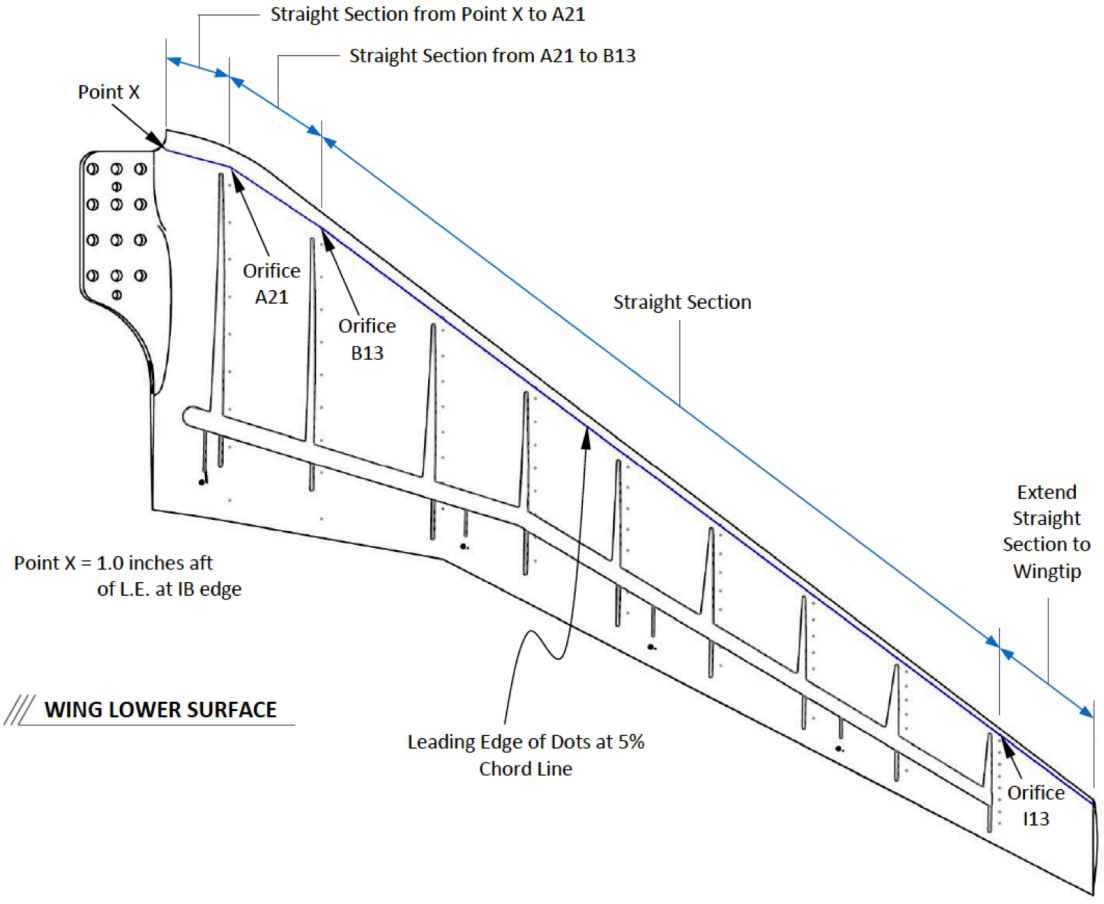


**Figure 5.1 Illustration of Trip Dot Locations on the Wing Lower Surface.**

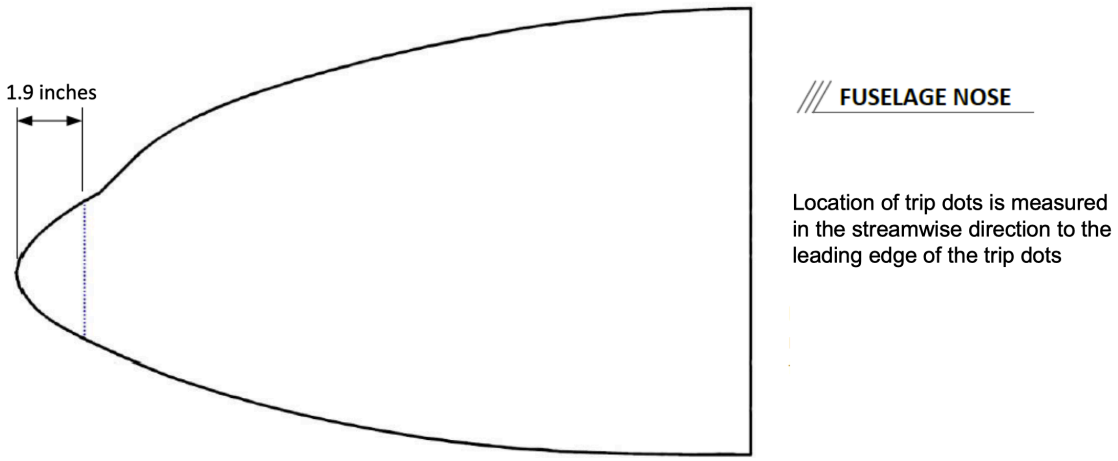


**Figure 5.2 Illustration of Trip Dot Locations on the Fuselage Nose.**

# 6. Static Pressure Instrumentation

There are nine streamwise rows of static pressure ports on the wing. The rows are distributed across the span of the wing as described in Tables 6.1 and 6.2 and illustrated in Figure 6.1. Note that the upper surface locations of the wire ports used for the carbon-based heating layer are also illustrated (black circles near trailing edge) in Figure 6.1. The semispan location values ($Y/Y_{tip}$) provided are based on the distance from the fuselage centerline to the wing tip (excluding rounded wing tip), and the X and Y values are based on the reference system used in the geometry files.

There are two pressure port layouts used, referred to as "Layout A" and "Layout B", as illustrated in Figure 6.2. The layouts differ in where the upper surface pressure ports begin. The first pressure port on Layout A is very near the leading edge (x/c=0.001), and the first pressure port on Layout B is at x/c=0.25. The lower surface pressure port locations are identical for both layouts. The distribution and locations of ports are described in Tables 6.3 and 6.4.

During testing, three pressure ports were identified as being plugged and have therefore been removed from the data files provided on the website. A list of the pressure ports removed from the data files is provided in Table 6.5.

**Table 6.1 Pressure Port Summary.**

| Model Surface | Number of Pressure Ports |
|---|---|
| Upper Surface | 140 |
| Lower Surface | 90 |
| Total | 230 |

**Table 6.2 Spanwise Location of Pressure Port Rows.**

| Row | $X_{LE}$ [in.] | $Y_{LE}$ [in.] | $Y/Y_{tip}$ | Chord [in.] | Layout |
|---|---|---|---|---|---|
| A | 54.627 | 9.782 | 0.163 | 21.778 | A |
| B | 58.327 | 15.144 | 0.252 | 19.022 | B |
| C | 63.743 | 22.256 | 0.370 | 14.861 | A |
| D | 67.865 | 27.670 | 0.460 | 13.535 | B |
| E | 71.988 | 33.083 | 0.550 | 12.210 | B |
| F | 76.110 | 38.497 | 0.640 | 10.885 | A |
| G | 80.232 | 43.910 | 0.730 | 9.560 | B |
| H | 84.354 | 49.324 | 0.820 | 8.235 | A |
| I | 88.476 | 54.738 | 0.910 | 6.909 | B |

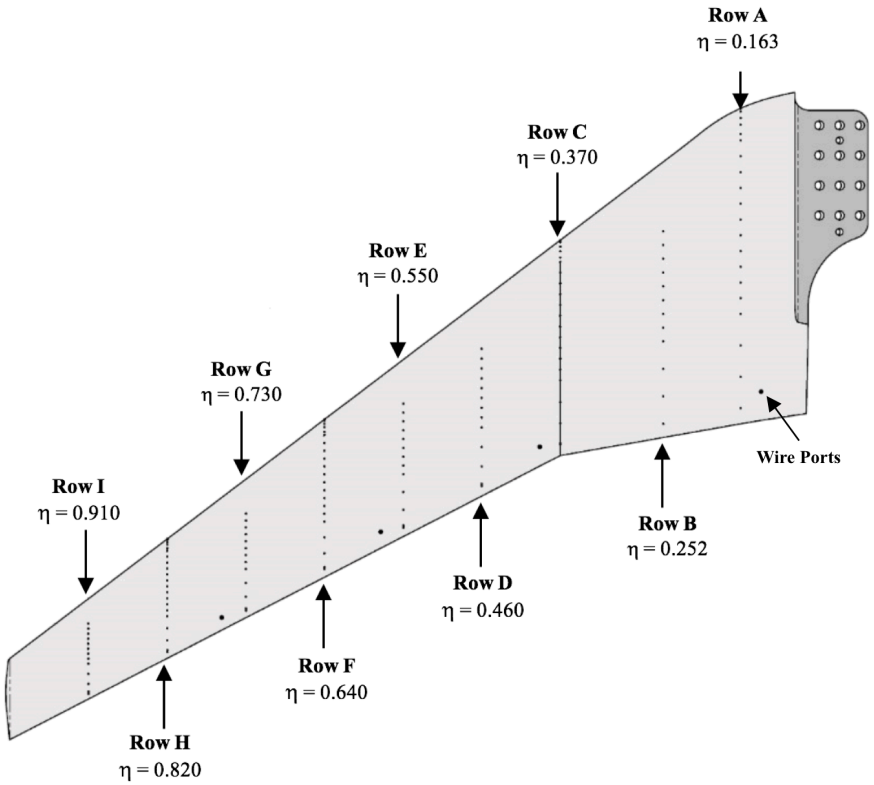


**Figure 6.1 Planform View of Wing Upper Surface Showing Pressure Port Rows.**

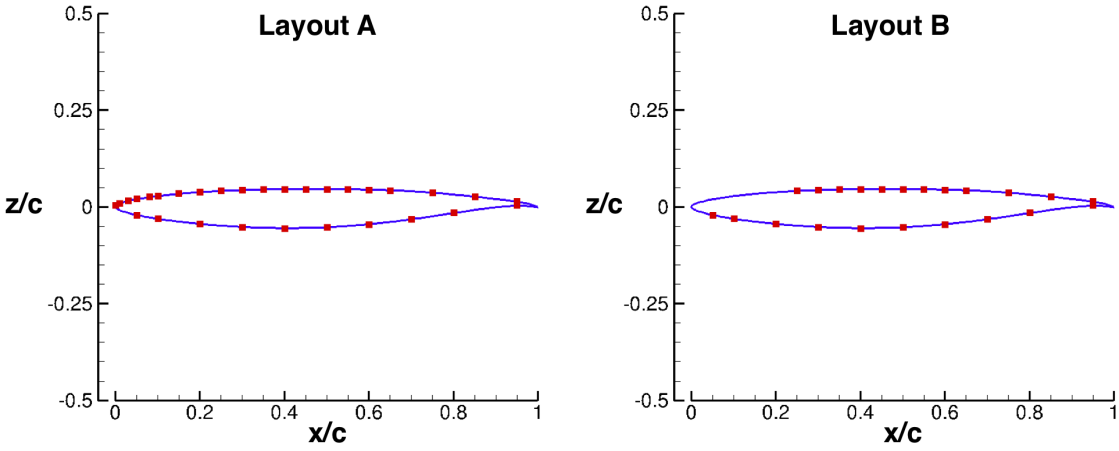


**Figure 6.2 Example of Layout A and B Pressure Port Distribution.**

**Table 6.3 Distribution of Pressure Ports per Layout.**

| LAYOUT A | | LAYOUT B | |
|---|---|---|---|
| Upper Surface | 20 | Upper Surface | 12 |
| Lower Surface | 10 | Lower Surface | 10 |
| Total | 30 | Total | 22 |

**Table 6.4 Port Number, Location, and Size of Pressure Ports per Layout.**

| LAYOUT A | | | | LAYOUT B | | | |
|---|---|---|---|---|---|---|---|
| **Port #** | **X/C** | **Surface** | **Size (ID) [in.]** | **Port #** | **X/C** | **Surface** | **Size (ID) [in.]** |
| 1 | 0.001 | Upper | 0.020 | 1 | 0.25 | Upper | 0.020 |
| 2 | 0.01 | Upper | 0.020 | 2 | 0.30 | Upper | 0.020 |
| 3 | 0.03 | Upper | 0.020 | 3 | 0.35 | Upper | 0.020 |
| 4 | 0.05 | Upper | 0.020 | 4 | 0.40 | Upper | 0.020 |
| 5 | 0.08 | Upper | 0.020 | 5 | 0.45 | Upper | 0.020 |
| 6 | 0.10 | Upper | 0.020 | 6 | 0.50 | Upper | 0.020 |
| 7 | 0.15 | Upper | 0.020 | 7 | 0.55 | Upper | 0.020 |
| 8 | 0.20 | Upper | 0.020 | 8 | 0.60 | Upper | 0.020 |
| 9 | 0.25 | Upper | 0.020 | 9 | 0.65 | Upper | 0.020 |
| 10 | 0.30 | Upper | 0.020 | 10 | 0.75 | Upper | 0.020 |
| 11 | 0.35 | Upper | 0.020 | 11 | 0.85 | Upper | 0.020 |
| 12 | 0.40 | Upper | 0.020 | 12 | 0.95 | Upper | 0.020 |
| 13 | 0.45 | Upper | 0.020 | 13 | 0.05 | Lower | 0.020 |
| 14 | 0.50 | Upper | 0.020 | 14 | 0.10 | Lower | 0.020 |
| 15 | 0.55 | Upper | 0.020 | 15 | 0.20 | Lower | 0.020 |
| 16 | 0.60 | Upper | 0.020 | 16 | 0.30 | Lower | 0.020 |
| 17 | 0.65 | Upper | 0.020 | 17 | 0.40 | Lower | 0.020 |
| 18 | 0.75 | Upper | 0.020 | 18 | 0.50 | Lower | 0.020 |
| 19 | 0.85 | Upper | 0.020 | 19 | 0.60 | Lower | 0.020 |
| 20 | 0.95 | Upper | 0.020 | 20 | 0.70 | Lower | 0.020 |
| 21 | 0.05 | Lower | 0.020 | 21 | 0.80 | Lower | 0.020 |
| 22 | 0.10 | Lower | 0.020 | 22 | 0.95 | Lower | 0.020 |
| 23 | 0.20 | Lower | 0.020 | | | | |
| 24 | 0.30 | Lower | 0.020 | | | | |
| 25 | 0.40 | Lower | 0.020 | | | | |
| 26 | 0.50 | Lower | 0.020 | | | | |
| 27 | 0.60 | Lower | 0.020 | | | | |
| 28 | 0.70 | Lower | 0.020 | | | | |
| 29 | 0.80 | Lower | 0.020 | | | | |
| 30 | 0.95 | Lower | 0.020 | | | | |

**Table 6.5 Removed Pressure Port Data.**

| Row | Port Location |
|---|---|
| B | Lower surface, x/c = 0.80 |
| H | Upper surface, x/c = 0.55 |
| I | Upper surface, x/c = 0.75 |

# 7. Semispan Model Standoff

A 2-inch nonmetric standoff was used to ensure that the metric model parts are immersed in the freestream flow and are not subjected to test section wall boundary layer effects. A labyrinth seal was used between the nonmetric standoff and the metric fuselage to block flow while preventing the metric break. The standoff is shown in the assembled model view in Figure 7.1, as well as Figure 2.1.

The standoff is not modeled in the CRM-NLF geometry file provided on the website.

Gap measurements were made between the metric fuselage and the nonmetric standoff, as well as between the nonmetric standoff and the wall. The average gap measurements between these surfaces are provided in Table 7.1.

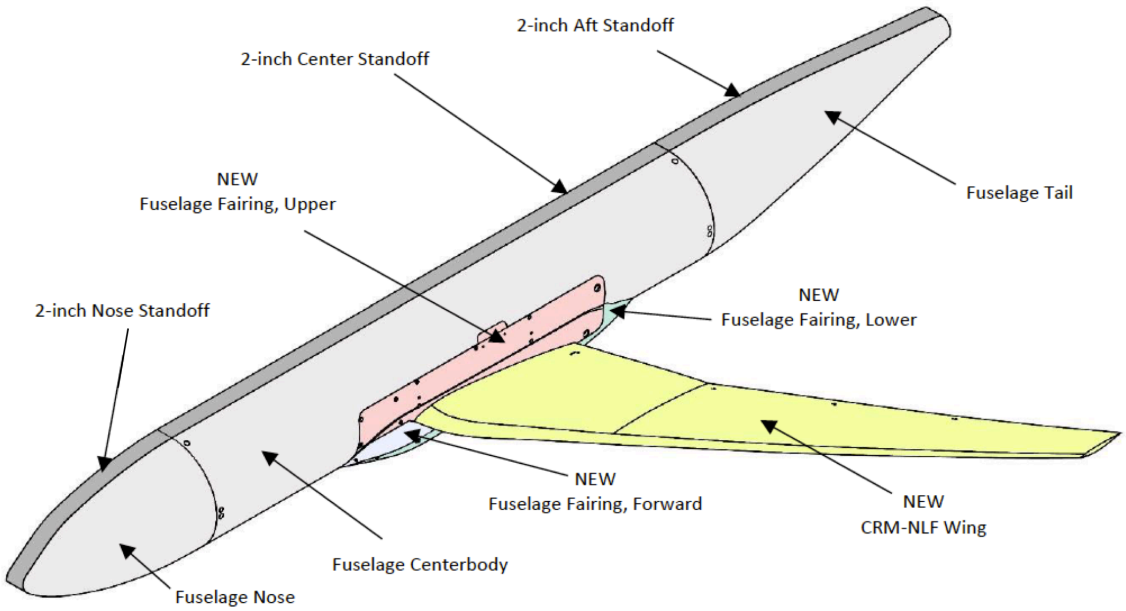


**Figure 7.1 View of Assembled Model and Components.**

**Table 7.1 Average Standoff Gap Measurements.**

| Surfaces | Average Gap Measurement [in.] |
|---|---|
| Fuselage to Standoff | 0.258 |
| Standoff to Tunnel Wall | 0.206 |

# 8. Data Correction Information

The dwell time for each data point on this website was 30 seconds, and the acquisition rate was 80 Hz. All data provided on the website have been conditionally sampled (via a Mach tolerance) and averaged. A Mach tolerance of +/- 0.001 was applied to the data, such that all frames with a measured Mach number within 0.001 of the setpoint Mach number would be included in the final average, and all frames outside that tolerance would be excluded. The data provided have been corrected for model blockage and wall interference using the Transonic Wall Interference Correction System, or TWICS, method. This methodology uses the measured wall pressures, model geometry, and tunnel conditions to calculate Mach, dynamic pressure, angle-of-attack, and balance corrections. These corrections were also applied to the surface pressure data provided on the website.

# 9. Freestream Disturbance Intensity Measurements

Flow quality measurements were acquired in the NTF following the CRM-NLF test to evaluate the disturbance levels in the test section at conditions specific to the CRM-NLF test. Flow surveys were acquired using a 7-foot survey rake that was populated with 21 sensor probes for mean and fluctuating measurements. Roll polar data were acquired to evaluate the spatial uniformity of the flow disturbance field. For the disturbance characterization, four hot-wire sensor probes and two unsteady pressure probes were used for these assessments.

All data presented here are for the Nitrogen-mode transonic conditions (Mach ≈ 0.86) relevant to the CRM-NLF test conditions. The root-mean-square (rms) total pressure fluctuations normalized by the total pressures, $<p'_t>/p_t$, are generally less than 0.1%. Similarly, the rms static pressure fluctuations normalized the dynamic pressure, $<p'_s>/q$, are less than 0.5%. Measured massflux intensities, $<(\rho u)'>/(\rho u)$, are in the range of 0.1 to 0.2% and turbulence intensities, $<u'>/u$, are less than 0.25%. These results are consistent with earlier Nitrogen-mode results obtained in 2011 before modifications were made to the flow path and demonstrate a spatially-uniform disturbance field. The conditions that the CRM-NLF experiment was conducted were found to have acceptable disturbance levels for testing of laminar flow configurations.